

Supporting Information

VIS-IR electrochromic device with electromagnetic wave absorption function based on PANI composite material

Shengwei Tang¹, Junlong Niu¹, Changle Gu³, HengZhi Zhang¹, Rongzong Zheng¹,
Xiaolong Weng^{1,2*}, Chunyang Jia^{1,2*}

¹ State Key Laboratory of Electronic Thin Films and Integrated Devices, School of Integrated Circuit Science and Engineering, University of Electronic Science and Technology of China, Chengdu 610054, P. R. China

² National Engineering Research Center of Electromagnetic Radiation Control Materials, School of Electronic Science and Engineering, University of Electronic Science and Technology of China, Chengdu 610054, P. R. China

³ Luzhou Laojiao Group Co., Ltd., Luzhou 646000, P. R. China

* Corresponding author: E-mail: cyjia@uestc.edu.cn

Fig. S1 Photo images of the structure of prepared devices.

Fig. S2 EDS-Mapping elemental analysis diagram of Fe₃O₄@PANI(2:1).

Fig. S3 Full spectrum XPS spectra of Fe₃O₄@PANI(2:1).

Fig. S4 Electromagnetic parameters of Fe₃O₄, Fe₃O₄@PANI, and PANI. (a) Real part of the dielectric constant ϵ' ; (b) Imaginary part of the dielectric constant ϵ'' ; (c) Tangent of the dielectric loss angle $\tan \delta\epsilon$; (d) Real part of the magnetic permeability μ' ; (e) Imaginary part of the magnetic permeability μ'' ; (f) Tangent of the magnetic loss angle $\tan \delta\mu$.

Fig. S5 The actual photo images of electrochromic devices with different voltages.

Fig. S6 (a) Visible light-near infrared reflectance curve of the device; (b) CIE L*a*b* color coordinates of the device. Stability and response time of the device (c) Infrared reflectance curve of the device; (d) Infrared emissivity curve of the device.

Fig. S7 FT-IR spectra of Fe₃O₄, Fe₃O₄@PANI, and PANI.

Fig. S8 SEM image of the (a) nylon membrane and (b) gold-plated membrane.

Fig. S9 (a) Nyquist plot of ECD. (b) The equivalent circuit of EIS curve.

Fig. S10 The variation of the optical density of the PANI as a function of charge density.

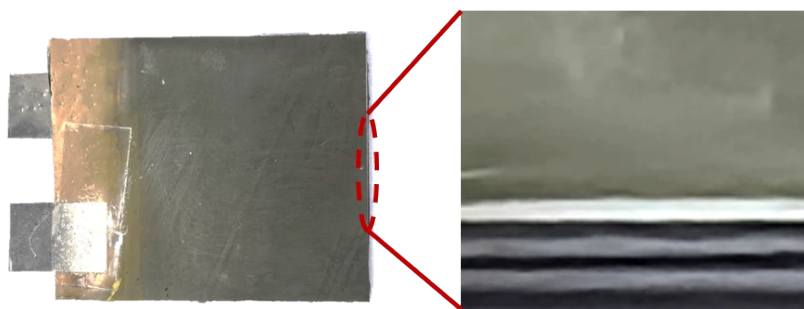


Fig. S1

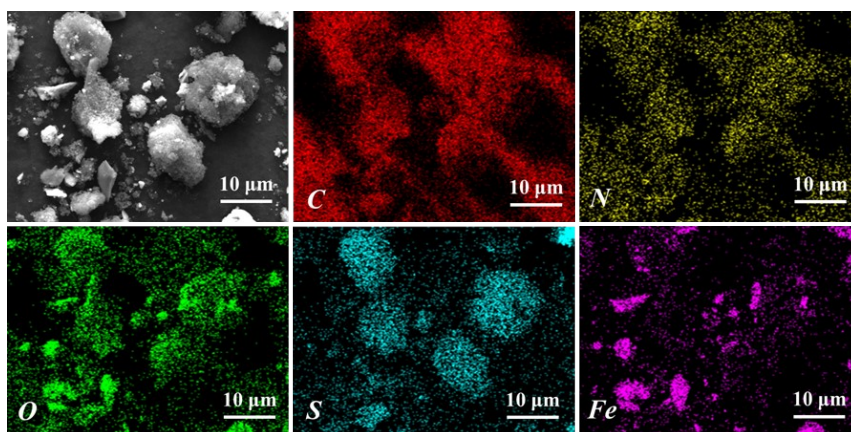


Fig. S2

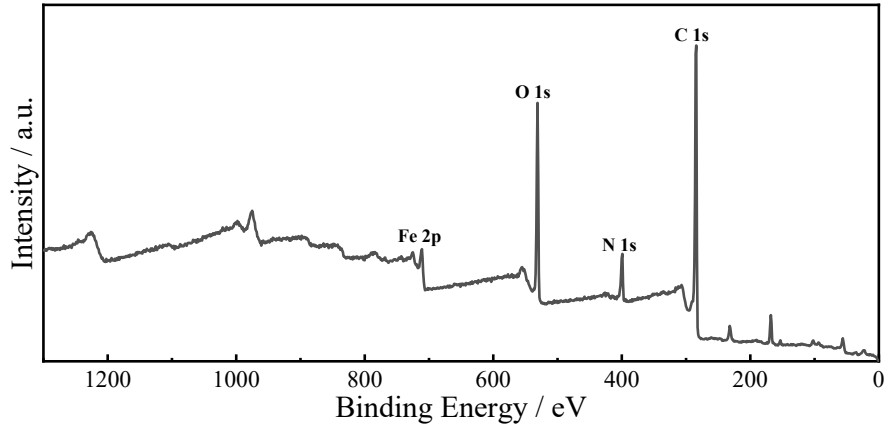


Fig. S3

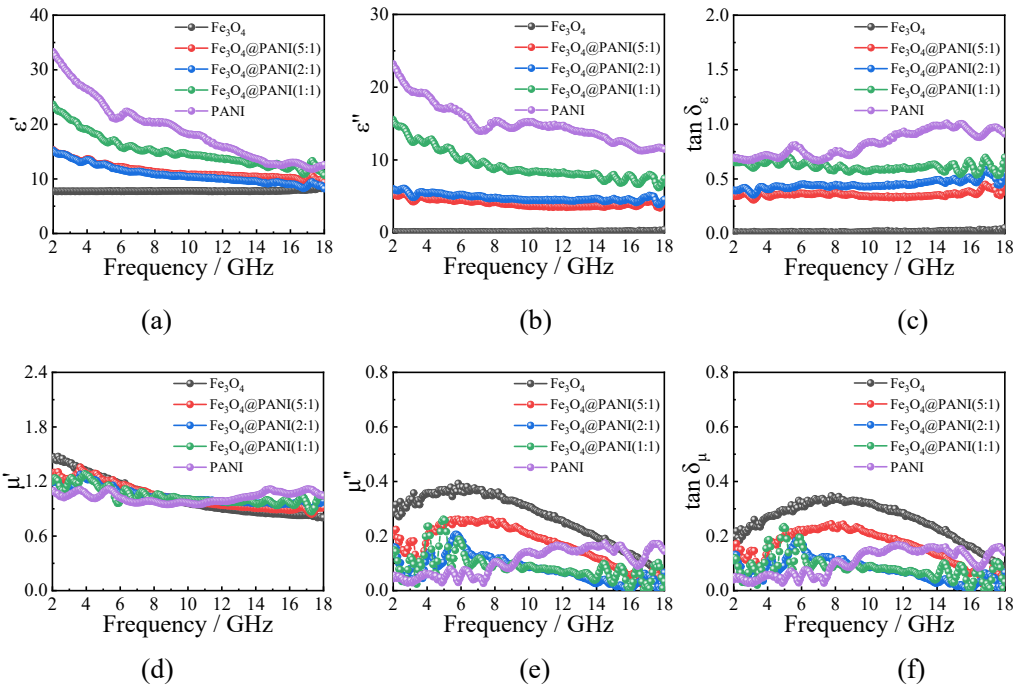


Fig. S4

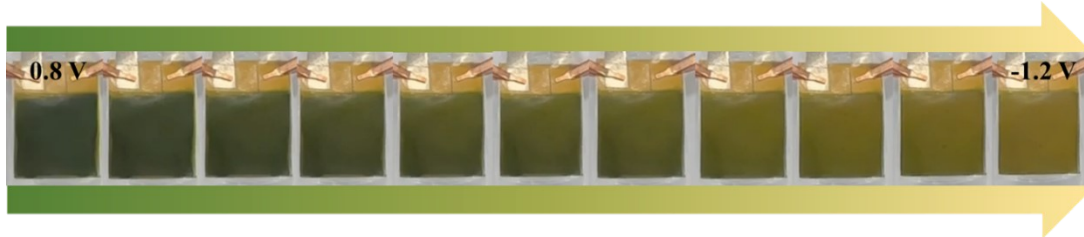


Fig. S5

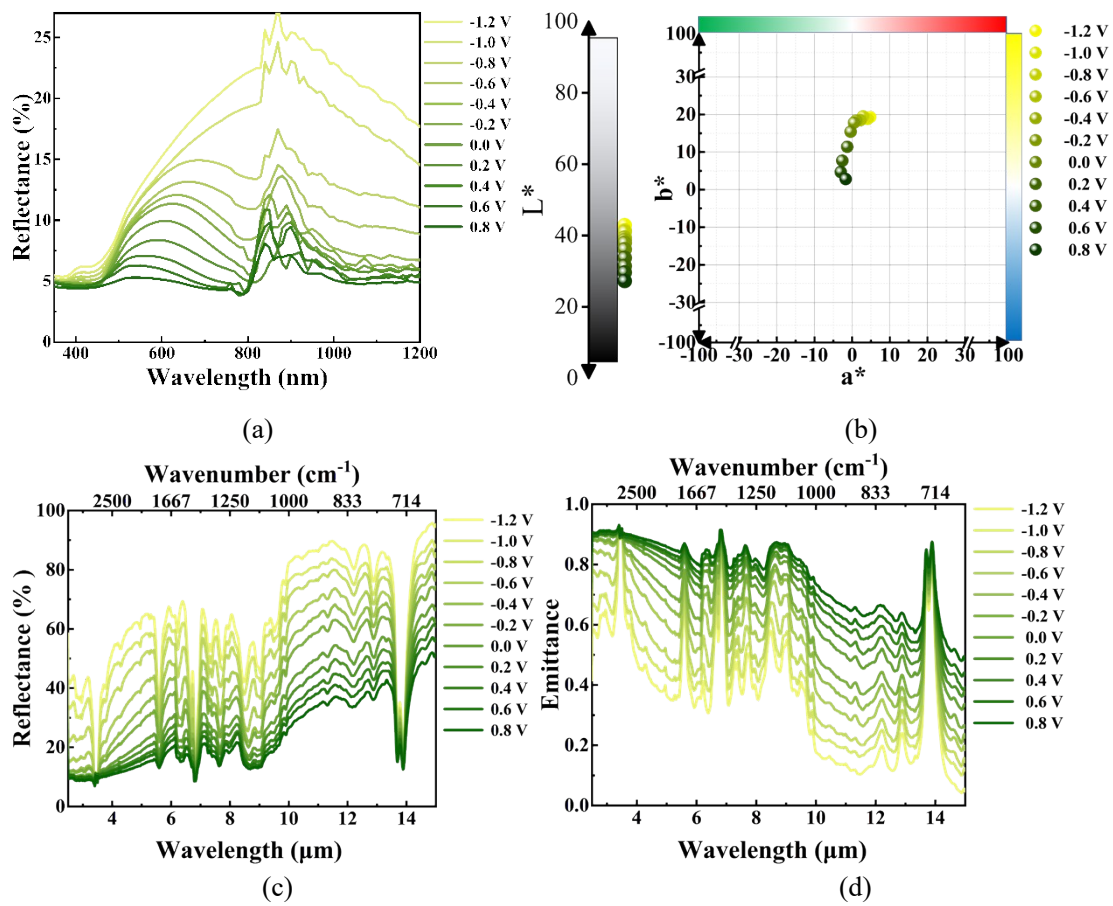


Fig. S6

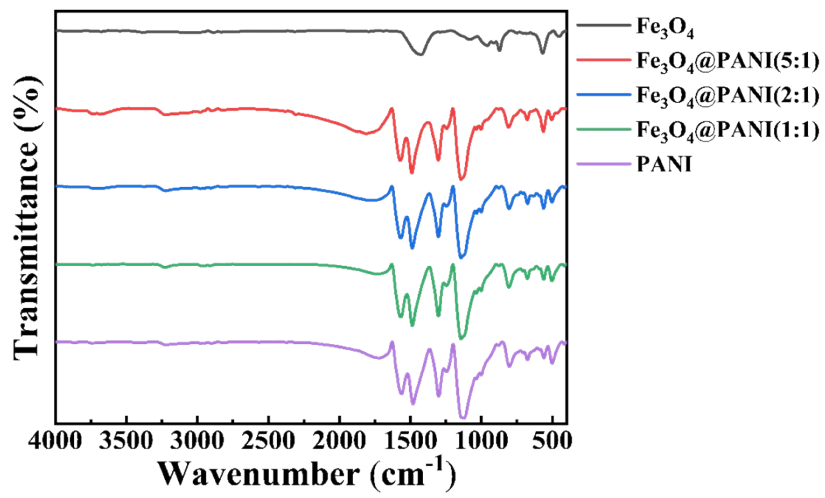
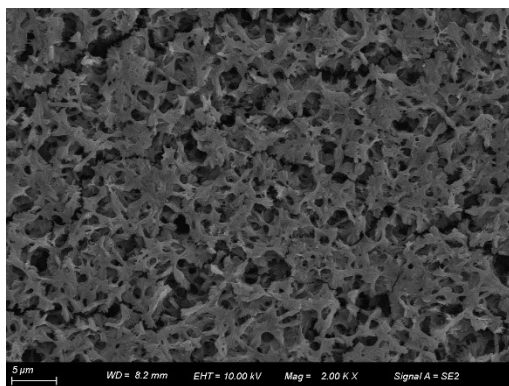
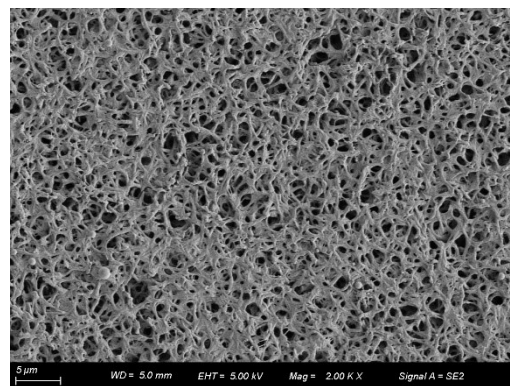


Fig. S7

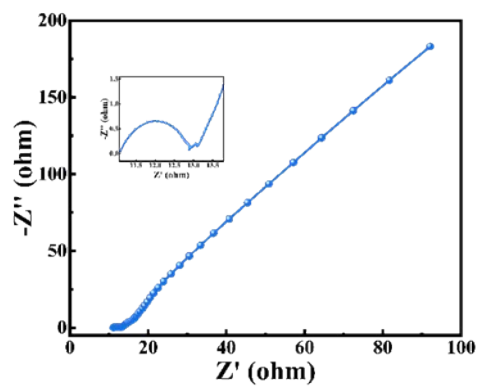


(a)

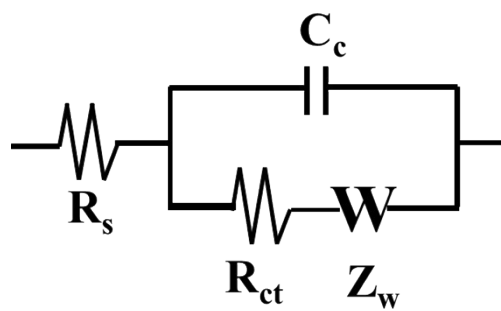


(b)

Fig. S8



(a)



(b)

Fig. S9

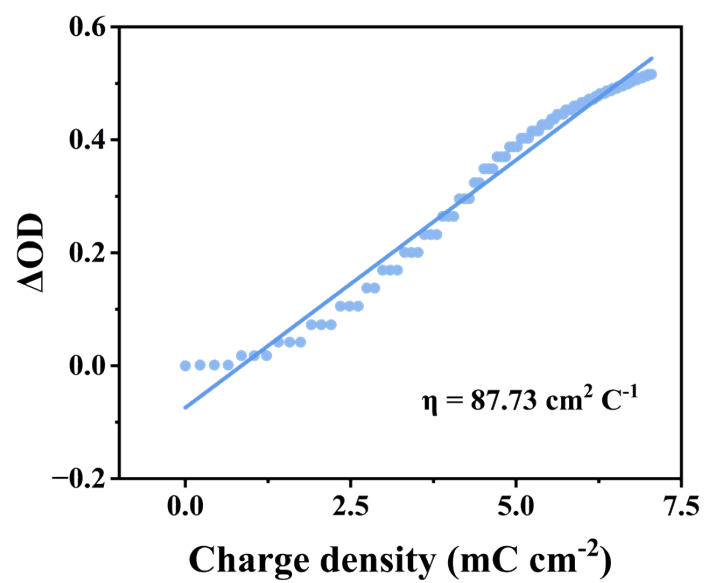


Fig. S10

Preparation of electrochromic working electrodes

Flexible porous conductive gold electrode preparation: A conductive layer of gold film with a thickness of about 300 nm was deposited on the surface of porous nylon film by electron beam deposition system. During the gold target deposition process, the vacuum in the chamber was reduced to below 3×10^{-3} Pa. The deposition rate was about 10 nm s⁻¹. The sheet resistance of the flexible porous conductive gold electrode was 54.3 mΩ cm⁻², and the maximum size could reach 40×50 cm². The electrode could be cut to the desired size according to the actual needs in the experiment.

Two-step electrochemical deposition of PANI film: The electrochemical deposition solution of PANI film was 1 M HClO₄ aqueous solution containing 0.1 M aniline. Ag/AgCl electrode and stainless-steel electrode were used as reference electrode and counter electrode, respectively. The first step of electrochemical deposition of PANI film was carried out by cyclic voltammetry in the potential range of 0-1.0 V for 5 cycles, with a scan rate of 50 mV s⁻¹. The second step of electrochemical deposition was carried out by constant current method at a current density of 0.25 mA cm⁻² for 2 h. After electrochemical deposition, the surface of PANI film was washed with deionized water and dried under vacuum at 60°C for 12 h.

Characterization of microporous gold-plated membrane

Scanning electron microscopy (SEM) analysis revealed the intricate structures of microporous nylon membranes and microporous gold films, as shown in Fig. S7(a) and (b). The SEM images displayed that the microporous nylon membrane consists of a tangled network of nylon fibers, forming numerous micrometer-sized pores. These micropores provide a larger surface area, endowing the nylon membrane with excellent surface properties. During the electron beam evaporation process, gold nanoparticles were uniformly deposited on the nylon fibers, creating a continuous metallic network. This unique structure endowed the microporous gold film with superior electrical conductivity. Even after metallization, the porous structure remained within the film, which is crucial for electrolyte storage. These pores not only increased the contact area between the electrolyte and the membrane but also enhanced the adsorption and storage efficiency of the electrolyte on the membrane. In electrochemical reactions, these porous structures could facilitate the rapid transport of ions, providing convenient pathways for ions to move quickly across the membrane surface. This aspect is critical for electrochemical reactions as it reduces the impedance between the electrolyte and the membrane and helps to increase the rate of reaction.

Fourier transform infrared analysis of Fe₃O₄@PANI

The Fig.S8 shows the FTIR spectra of Fe₃O₄, PANI, and Fe₃O₄@PANI. Fe₃O₄ exhibits an absorption peak for Fe-O stretching vibration at 570 cm⁻¹; PANI shows new vibrational peaks at 1577, 1487, 1305, and 1143 cm⁻¹, which are respectively attributed to the absorption peaks of C=C stretching vibrations of the quinoid ring structure units, C=C stretching vibrations of the benzene ring structure units, C-N stretching vibrations of the benzene ring structure units, and C=N stretching vibrations of the quinoid ring structure units. Fe₃O₄ @PANI also possesses the aforementioned absorption peaks.

Electrochemical impedance spectroscopy analysis of ECD

Electrochemical impedance spectroscopy (EIS) testing was conducted on electrochromic devices. The amplitude of AC was maintained to 5 mV and the frequency range was from 100 KHz to 0.01 Hz. Fig.S9(a) show the Nyquist plots of the ECD. It is generally believed that in the EIS curve, the semicircle in the high-frequency region corresponds to the charge-transfer impedance between the electrode and the electrolyte, and the slope of the straight line in the low-frequency region is related to the ion diffusion process. Fig. S9(b) shows the equivalent circuit of the EIS curves, where R_s , R_{ct} , C_c and Z_w represent the system resistance, charge-transfer resistance, membrane capacitance and Warburg impedance in the electrochemical system, respectively. The smaller size of the semicircle in the EIS curve reflects the lower charge transfer resistance of the device.

The coloring efficiency of PANI thin films

Using a method akin to that employed for crafting working electrodes on porous gold substrates, PANI thin layers were deposited on ITO surfaces. The electrochromic attributes of the PANI coatings were assessed by examining their coloration efficiency. This metric gauges the alteration in visible light transmittance per unit of electric charge consumed over a given area, as delineated by the equation (

$$\eta = \frac{\Delta OD}{\Delta Q} = \frac{\log_{10}\left(\frac{T_b}{T_c}\right)}{\Delta Q}$$
). The coloration efficiency reflects the rate at which the electrochromic material's optical properties can be modified. Typically, a greater coloration efficiency signifies a more effective electrochromic substance, implying that minimal charge is needed to modify light transmittance. Here, ΔOD denotes the variation in optical density, while ΔQ indicates the charge density shift necessary for this optical change, determined via chronoamperometry. Referencing Fig. S10, the points for ΔOD and ΔQ at various intervals are plotted, and the coloration efficiency (η) is derived from the gradient of the linear portion of these points. Experimental findings reveal that the PANI layer's coloration efficiency stands at 87.73 cm²/C.